

Energy Window Selection for Bremsstrahlung ^{90}Y SPECT-CT Imaging: A Phantom Study

Denise Curto¹, Faustino Bonutti², Youssef Bouzekraoui³, Farida Bentayeb⁴, Hicham Asmi⁴

1. Physics Department, University of Trieste, Italy
2. Academic Hospital of Udine, Medical Physics Department, Italy
3. Hassan First University of Serrat, High Institute of Health Sciences, Laboratory of Sciences and Health Technologies, Serrat, Morocco
4. Department of Physics, LPHE, Modeling and Simulations, Faculty of Science, Mohammed V University, Rabat, Morocco

ARTICLE INFO

Article type:
Original Paper

Article history:
Received: Aug 15, 2020
Accepted: Feb 14, 2021

Keywords:
Bremsstrahlung
Yttrium-90
NEMA IEC PET Body
Phantom
ISO-Counting Curves

ABSTRACT

Introduction: In Yttrium-90 SPECT imaging, the energy window and collimator used during projection acquisition can significantly affect image quality. In this work, we used a new and independent method to verify previous results, which suggest suitable energy around 130 keV.

Material and Methods: We used Siemens Symbia SPECT-CT system fitted with High Energy General Purpose (HEGP), Medium Energy General Purpose (MEGP), and Low Energy High Resolution (LEHR) to acquire data from NEMA IEC PET Body Phantom filled with ^{90}Y chloride. ISO-counting curve is a new method analysed in this study to evaluate the adequate parameters for ^{90}Y SPECT imaging.

Results: HEGP collimator was the most suitable for acquisitions of ^{90}Y bremsstrahlung radiation from the point of view of the correct volume reproduction. ISO-counting analyses have shown that for the bigger phantom spheres, the optimum acquisition energy is centered on 130 keV.

Conclusion: The ISO-counting curve method is consistent to previous studies' results and can help to improve image quality.

► Please cite this article as:

Curto D, Bonutti F, Bouzekraoui Y, Bentayeb F, Asmi H. Energy Window Selection for Bremsstrahlung ^{90}Y SPECT-CT Imaging: A Phantom Study. Iran J Med Phys 2022; 19: 43-48. 10.22038/IJMP.2021.51256.1837.

Introduction

Intrahepatic transarterial radioembolization is a type of therapy indicated for liver malignancies, consisting of a surgical injection of Yttrium-90 microspheres inside the hepatic vein. This is possible due to the liver anatomy: in the case of a healthy liver, the portal vein supplies 70-80% of the blood to the liver, while liver tumours such as hepatocellular carcinoma (HCC) receive 80-100% of its blood from the hepatic vein. [1].

The post-treatment imaging, may be carried out with time-of-flight (TOF) PET (Positron Emission Tomography) [2] or SPECT (Single Photon Emission Computed Tomography) to verify the correct positioning of the Yttrium-90 microspheres inside the patient. The TOF PET is usable because the ^{90}Y nucleus emits 32 positrons per second per MBq with a maximum energy of 758 keV [3-4]. Regarding the SPECT imaging, it is not possible using the conventional methods, that involve the use of γ -emitter radioisotopes, whose spectrum has one or more photoemission peaks that allow selecting an energy range useful for the acquisition.

The high energy electrons from the ^{90}Y decay, interact with tissues and produce bremsstrahlung radiation. The bremsstrahlung spectrum detected by the imaging system scintillator is continuum without

the photopeaks, so it does not allow to identify a suitable energy window for the projection acquisition and prevents from distinguishing between the primary photons and the Compton photons. It is necessary to establish a data acquisition method with optimized energy window and acquisition parameters in order to be used for the post-therapy SPECT acquisition.

A number of studies have been reported on selecting the appropriate collimator and energy window setting for bremsstrahlung imaging. S. Heard et al. used Monte Carlo to simulate Bremsstrahlung radiation from ^{90}Y point sources to accurately model to investigate optimal imaging parameters. They reported that the highest image contrast was achieved with medium energy collimators at 100-150 keV [5]. X. Rong et al. developed a new method for optimizing the acquisition energy window and found that an optimal energy window was in the range of 100-160 keV [6]. O. S. Huey et al. found in a phantom study that the best signal to background ratio was obtained using energy windows centered around the 80 and 120 keV [7]; Y. Bouzekraoui et al. showed in their Monte Carlo simulations that the energy window in the range of 120 to 150 keV maximize the contrast to noise ratio in the ^{90}Y bremsstrahlung SPECT imaging [8]. C. A. Porter

et al. evaluated the energy window of 50-130 keV in the post-therapy SPECT/CT imaging of ^{90}Y microspheres delivered to hepatic malignancies [9]. M. Kim et al. also used Monte Carlo simulations with different collimators and energy window set-up ranging from 50 to 400 keV in order to optimize ^{90}Y bremsstrahlung images [10]. All these studies proposed optimal energy windows in the range of 130 keV.

The aim of this study is to propose a new method to select the most suitable energy window for ^{90}Y SPECT imaging, using the ISO-counting curves acquired from NEMA IEC PET Body Phantom filled with ^{90}Y chloride.

Materials and Methods

This phantom study was performed using the NEMA IEC PET Body Phantom with 6 fillable spheres having inner diameters of 3.7, 2.8, 2.2, 1.7, 1.3, 1.0 cm (Figure 1).



Figure 1. NEMA IEC PET Body Phantom

Dimensions of the two larger spheres were suitable for simulating liver malignancies, which in our center (Udine University hospital) were observed of an average diameter of 3.4 cm for 38 patients treated for HCC.

The phantom was filled with ^{90}Y chloride solution in order to obtain a homogeneous activity distribution. The ^{90}Y chloride solution was preferred over the ^{90}Y microspheres, because they suddenly fell down to the bottom of the phantom and do not provide a uniform activity distribution within the volume.

Eight SPECT-CT images were acquired from the phantom. In four of the phantom images, only the spheres were filled with ^{90}Y Chloride solution, while the

phantom's background compartment was filled with water. In the other four images, the solution was also emptied into the phantom's background compartment. All the activity concentrations emptied into the spheres and background, and the SPECT-CT parameters are listed in Table 1, and Table 2, respectively.

It was possible to choose between three types of collimators set, each of them suitable for a different energy range: High Energy General Purpose (HEGP), Medium Energy General Purpose (MEGP), and Low Energy High Resolution (LEHR).

The gantry of the SPECT system could resolve in a circular or non-circular orbit, following phantom contours. Images were always acquired with a matrix of 256×256 pixels, except the sixth image obtained using a matrix of 128×128 pixels. The acquisition time for each projection (s/view) was another parameter that could be selected, according to the statistics of the counts required.

Table 1. Activity concentrations of ^{90}Y in the spheres (C_s) and background (C_b) of the NEMA IEC PET Body phantom for the eight different acquisition parameters (Table 2).

SET	C_s (MBq/mL)	C_b (MBq/mL)
1	3.374	-
2	3.322	-
3	2.627	-
4	2.586	-
5	1.192	0.153
6	1.167	0.150
7	0.920	0.118
8	0.695	0.089

Siemens Symbia SPECT-CT system allows selection of up to six simultaneous energy acquisition windows. Two different sets were chosen in the current study: one set with six narrow energy windows ranging from 50 keV to 196 keV, and the other set with six larger energy windows covering the region of 40-440 keV. In both cases, sub-windows are contiguous; their energy size and central positions are reported in Tables 3 and 4. OSEM Flash 3D iterative algorithm was used for image reconstruction.

Table 2. The parameter settings for the SPECT-CT acquisitions of the NEMA IEC PET Body phantom filled with ^{90}Y chloride.

SET	Windows	Collimator	Orbit	Matrix	s/view
1	narrow	HEGP	circular	256×256	180
2	large	HEGP	circular	256×256	120
3	narrow	HEGP	not circular	256×256	180
4	large	HEGP	not circular	256×256	120
5	large	HEGP	not circular	256×256	240
6	large	HEGP	not circular	128×128	240
7	large	MEGP	not circular	256×256	360
8	large	LEHR	not circular	256×256	360

Table 3. Energy size and central position of sub-windows in the narrow window-set.

Narrow sub-windows						
Sub-windows	NE1	NE2	NE3	NE4	NE5	NE6
Size (keV)	24.8	23.2	24.2	24.3	24.0	23.9
Center (keV)	62	86	110	135	160	184

Table 4. Energy size and central position of sub-windows in the large window-set.

Large sub-windows						
Sub-window	LE1	LE2	LE3	LE4	LE5	LE6
Size (keV)	59.5	58.5	58.9	60.0	80.0	80.0
Center (keV)	70	130	190	250	320	400

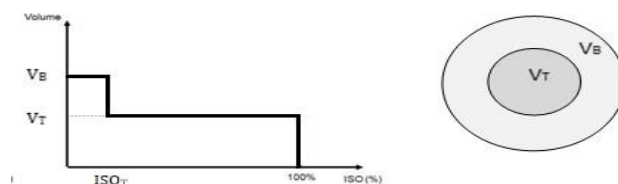


Figure 2. Ideal ISO-counting curve corresponding to a uniform activity distribution of a tumour volume V_T within a uniform background volume V_B . ISO_T threshold selects all the voxels within V_T . In our case, the tumour volume is represented by the phantom spheres.

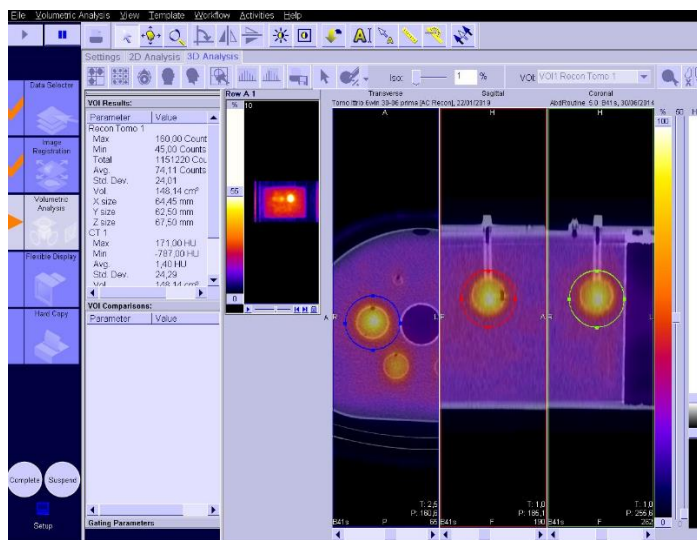


Figure 3. Symbia Siemens SPECT-CT software's home screen. Software tools allow drawing VOI around spheres on phantom's 3D images. On the left, there is a box that show data about VOI's counts and volume.

In order to find the proper energy ranges which optimizes the bremsstrahlung image, ISO-counting curves were reconstructed. These curves represent the volume of interest (VOI) as a function of the ISO% threshold. ISO% is a percentage value respect to the maximum of counts inside the VOI and setting ISO% threshold on Symbia Siemens SPECT-CT software allows to select all the voxels with a number of counts between the set ISO% threshold and the maximum. Figure 2, represents an ideal ISO-counting curve of a uniform activity distribution over a tumour volume (V_T) within a background volume (V_B).

Many factors make the real ISO-counting curves different from the ideal one, including physical

phenomena such as photon scattering and attenuation and imaging parameters such as the finite pixel size of the acquisition matrix. Our idea is that the energy window can be optimize to achieve the highest similarity between real and ideal ISO-counting curves. In particular, the best curve will be the one that best describes the sudden decrease of volume in correspondence to ISO_T (Figure 2).

ISO-counting curves were calculated for the three biggest spheres: a VOI was drawn around each sphere, and varying the ISO% threshold, the corresponding volume was provided by the software (Figures 3 and 4). ISO-counting curves were reconstructed for all the central sub-windows energy.

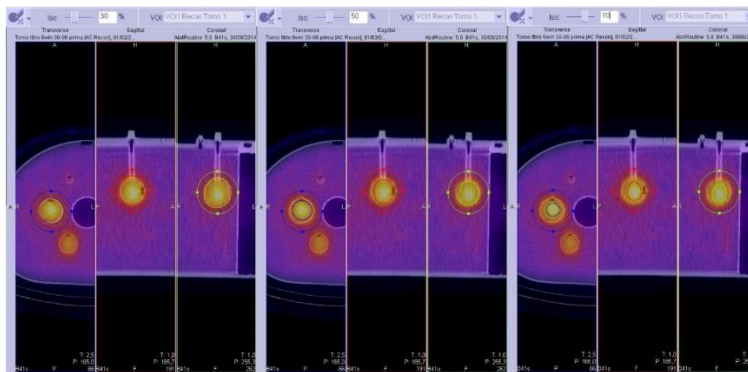


Figure 4. VOI sizes as function of ISO threshold, equal to 30% (left), 50% (centre) and 70% (right). VOI's volume shrinks (internal contours) when the ISO% value increases.

Results

Several phantom's images have been studied. More attention was paid to the 5th and 7th acquisition set (Table 2): large windows energy set, non-circular orbit and matrix with 256×256 pixels. The two acquisitions stand out because of the different collimators used, HEGP for the first one and MEGP for the second one. The bigger sphere's ISO-counting curves are shown in Figure 5 for the fifth acquisition and in Figure 6 for the seventh acquisition.

Each curve matches to an energy window. The lowest curve has the most similar ideal-trend of Figure 2; this is true for the curve related to the energy range centered in 130 keV. This result was obtained also analyzing the

acquisitions characterized from the third and fourth parameters set.

Comparing ISO-counting curves obtained from the fifth and seventh acquisition sets (Figure 7), it is possible to establish that the HEGP collimator is more suitable than the MEGP collimator for acquisitions of ⁹⁰Y bremsstrahlung radiation from the point of view of the correct volume reproduction.

Finally, ISO% values that better reproduce the sphere's volume have been determined by a linear interpolation starting from ISO-counting curves. Results from the third acquisition are reported in Table 5. Between ISO 30% and 50%, the true sphere's volume can be reproduced.

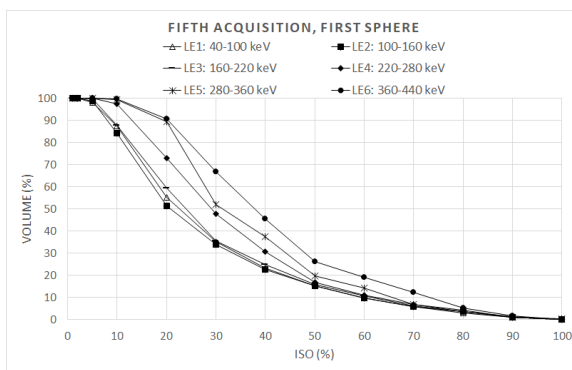


Figure 5. ISO-counting curves obtained analysing the biggest sphere acquired with parameters of the fifth acquisition: HEGP collimator, not circular orbit, matrix of 256 × 256 pixels, and 240 s/view. LE1, LE2, LE3, LE4, LE5, LE6 are the energy sub-windows of the large windows set (Tab.4).

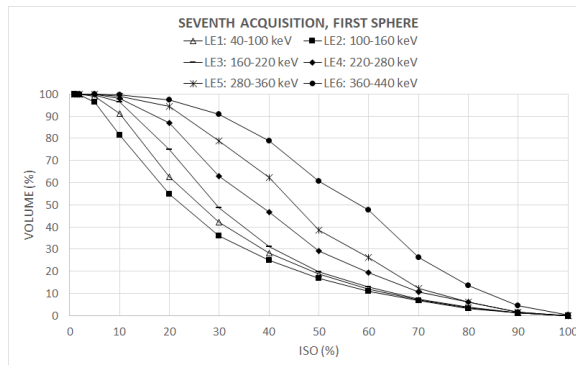


Figure 6. ISO-counting curves obtained analysing the biggest sphere acquired with parameters of the seventh acquisition: MEGP collimator, not circular orbit, matrix of 256 × 256 pixels, and 360 s/view. LE1, LE2, LE3, LE4, LE5, LE6 are the energy sub-windows of the large windows set (Tab.4).

Table 5. ISO% values obtained with linear interpolation that reproduce the real volume of the spheres for each energy sub-windows in the narrow windows set (Tab.3).

	Sub-Window	NE1	NE 2	NE 3	NE 4	NE 5	NE 6
ISO%	Sphere 1	31	32	30	30	33	34
	Sphere 2	39	37	36	33	34	39
	Sphere 3	47	47	45	47	47	54

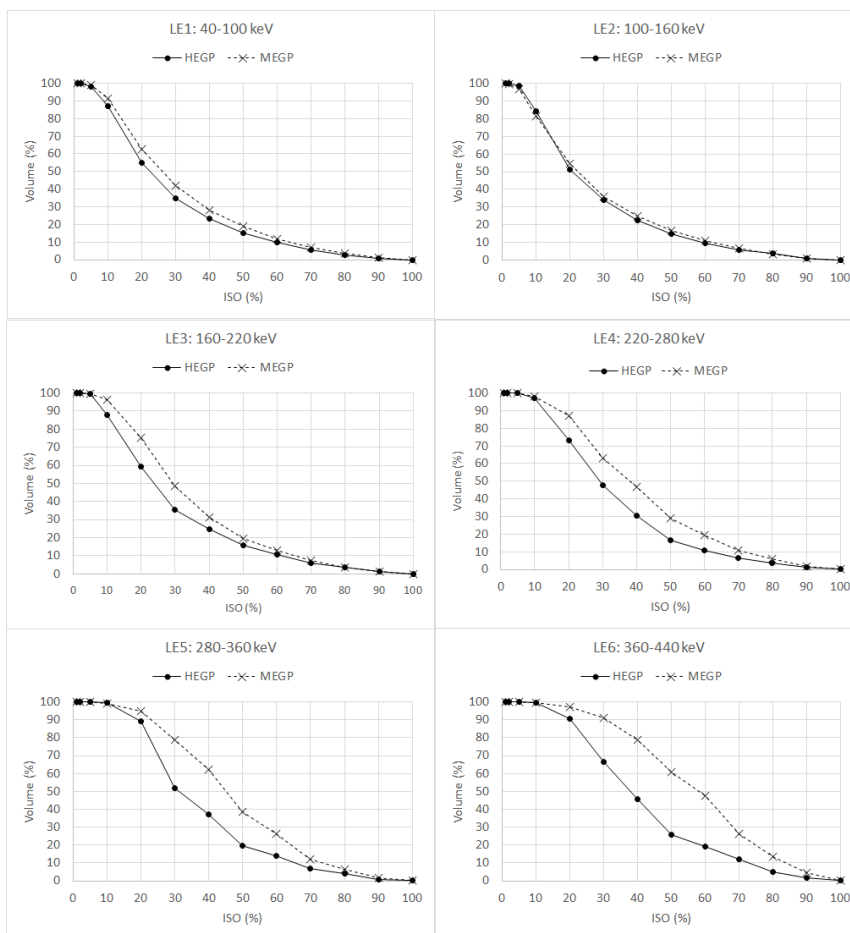


Figure 7. Comparison between ISO-counting curves obtained from fifth (HEGP collimators) and seventh (MEGP collimators) acquisitions sets. LE1, LE2, LE3, LE4, LE5, LE6 are the energy sub-windows of the large windows set (Tab.4).

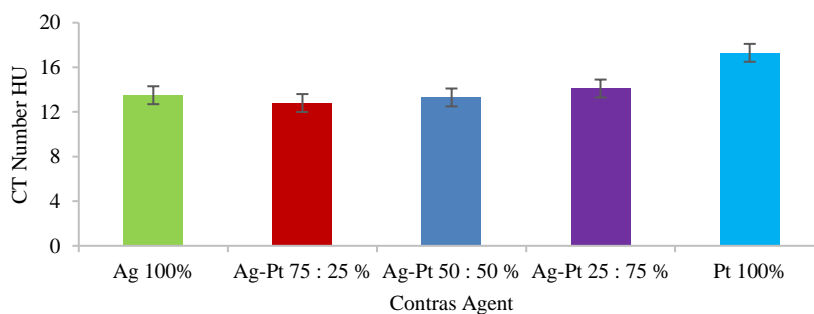


Figure 9. CT Scan tests on contrast properties of 100% AgNPs, 75%:25% Ag-PtNPs, 50%:50% Ag-PtNPs, 25%:75% Ag-Pt NPs, and 100% PtNPs

Discussion

For SPECT bremsstrahlung, imaging with ⁹⁰Y the choice of energy window is essential in order to

optimize the acquisition parameters. Different acquisition sets of the NEMA IEC PET Body phantom were analysed and a new method based on ISO-counting curve was proposed to determine the optimum energy

window. As shown in Figures 5 and 6, the curve with the most similar ideal-trend is that relative to energy window centered at 130 keV and size of 58.5 keV (LE2).

In order to establish the most suitable collimator for ^{90}Y SPECT imaging, a comparison between curves obtained with fifth and seventh acquisition parameters sets was performed for each energy window. Figure 7 shows that the ISO-counting curves relative to the HEGP collimator have the most similar ideal trend in all six graphs. The optimum window obtained by the ISO-counting curve is centred at 130keV with the HEGP collimator.

The ISO-counting curve method was used for the first time to determine the optimum energy window for ^{90}Y SPECT imaging, but results obtained in this study confirm those obtained from previous studies on contrast and Monte Carlo simulation [8].

The ISO-counting curve method was effective for reproducing the volumes of the spheres. For this purpose, the third acquisition (Tab.2) was chosen because the phantom in this case, was prepared without radioactivity in the background, more similar to a real patient case, and the narrow windows setup was selected. With a linear interpolation of the ISO-counting curves obtained from this acquisition, the ISO% values that reproduce the true volume of the spheres was estimated and reported in Table 5.

Further studies may be developed in the future to consolidate the ISO-counting curve method and establish the width of the optimum energy window for ^{90}Y SPECT imaging. The width of the energy window for the ^{90}Y acquisition can be established according to required counting statistics.

Conclusion

ISO-counting curve method is proposed to optimize ^{90}Y bremsstrahlung SPECT imaging. We found that the optimum energy window obtained by the ISO-counting curve is centred at 130keV with HEGP collimator, and these results are coherent with the previous literature.

The width of the optimal energy acquisition window can be established according to required counting statistics. In our department for radioembolization treatments with ^{90}Y micro-spheres, SPECT-CT acquisitions are made in the energy range between 100keV and 200keV, divided into five equal sub-windows.

The main limitation of our study is that it was not possible to correct the acquired data for scattering since the spectrum of photons emerging from the patient and measured by a gamma-camera detector has no photopeaks and the traditional methods for scatter radiation correction (i.e. dual or triple energy windows) are not applicable.

It can be expected that the scattering correction is important given the rather high energy of the bremsstrahlung radiation. An improvement in this direction could be the next step for future experiments, both by looking through Monte Carlo simulations for

the energy of acquisitions which minimize the impact of scattering, and developing algorithms for the raw data correction.

References

1. C. Breedis and G. Young, The blood supply of neoplasms in the liver, *Am. J. Pathol.* 30, 969–984 (1954)
2. R. Lhommel, L. van Elmbt, P. Goffette, M. Van den Eynde, F. Jamar, S. Pauwels, S. Walrand, Feasibility of (^{90}Y) TOF PET-based dosimetry in liver metastasis therapy using SIR-Spheres, *Eur J Nucl Med Mol Imaging* 37: 1654–1662 (2010)
3. H. Langhoff, H. H. Hennies, Zum Experimentellen Nachweis Von Zweiquantenzerfall Beim $0+0+\text{Ubergang}$ des $\text{Zr}90$, *Z Phys A At Nucl* 164: 166–173 (1961)
4. R. J. Nickles, A. D. Roberts, J. A. Nye, A. K. Converse, T. E. Barnhart, M. A. Avila-Rodriguez, R. Sundaresan, D. W. Dick, R. J. Hammas and B. R. Thomadsen, Assaying and PET imaging of yttrium-90: $1/\text{spl Gt}/34\text{ppm} > 0$, *IEEE Symposium Conf Record Nuclear Science* 3412–3414 (2004)
5. S. Heard, G. D. Flux, M. J. Guy, R. J. Ott, Monte Carlo Simulation of ^{90}Y Bremsstrahlung Imaging, *Nuclear Science Symposium Conference Record: IEEE.* 6, 3579-3583 (2004)
6. X. Rong, Y. Du, E. C. Frey, A method for energy window optimization for quantitative tasks that includes the effects of model mismatch on bias: application to Y-90 Bremsstrahlung SPECT imaging, *Phys. Med. Biol.* 57, 3711-3725 (2012)
7. O. S. Huey, Y. J. See, S. Nabila, H. S. Ping, I. Suzanah, Collimator and energy window optimization for practical imaging protocol and quantification of Yttrium-90 bremsstrahlung spect/ct: A phantom study, *Radiation Physics and Chemistry* 178 (2021) 109080
8. Y. Bouzekraoui, F. Bentayeb, H. Asmi, F. Bonutti, Energy window and contrast optimization for single-photon emission computed tomography bremsstrahlung imaging with yttrium-90. *Indian J Nucl Med* 2019;34:125-8.
9. C. A. Porter, K. M. Bradle, E. T. Hippeläinen, M. D. Walker and D. R. McGowan, Phantom and clinical evaluation of the effect of full Monte Carlo collimator modelling in post-SIRT yttrium-90 Bremsstrahlung SPECT imaging, *EJNMMI Research* (2018) 8:7 DOI 10.1186/s13550-018-0361-0
10. M. Kim, J. K. Bae, B. H. Hong, K. M. Kim, W. Lee, Effects of collimator on imaging performance of Yttrium-90 Bremsstrahlung photons: Monte Carlo simulation, *Nuclear Engineering and Technology*, 2018.